Supporting Information

Solution blow spinning of elastic 3D complex ZrO_2@Mullite nanofibrous aerogels toward customized thermal insulation

Wenlu Zhang [a], Mengzhe Bao [b], Mengyao Chen [c], Wenbin Li [a,b,*], Weilin Xu[a,*], Chong He [a,b,*]

a State Key Laboratory of New Textile Materials and Advanced Processing Technologies, Wuhan Textile University, Wuhan, Hubei 430200, China

b School of Textile Science and Engineering, Wuhan Textile University, Wuhan, Hubei 430200, China

c School of Foreign Languages, Wuhan Textile University, Wuhan, Hubei 430200, China

[*]**Corresponding author**

E-mail address: Wenbin_li@wtu.edu.cn (Prof. W. Li); weilin_xu@wtu.edu.cn(Prof. W. Xu); chhe@wtu.edu.cn (Ph. D Chong He)

Supplementary Discussions

Supplementary Figures S1 to S18

Supplementary Discussions

As shown in Figure S1, n-Propyl zirconate had a partial toughening effect for precursor solution. The optimal spinning viscosities were observed with the mullite precursor solution at 7.5 wt% and the ZrO_2/Mullite precursor solution at 6 wt%. As shown in Figure S2, the precursor mullite fiber and ZrO_2@Mullite nanofibers were dense and lightweight. The precursor cotton displayed a porous and dense structure, providing a foundational basis for subsequent investigations.

Supplementary Figures

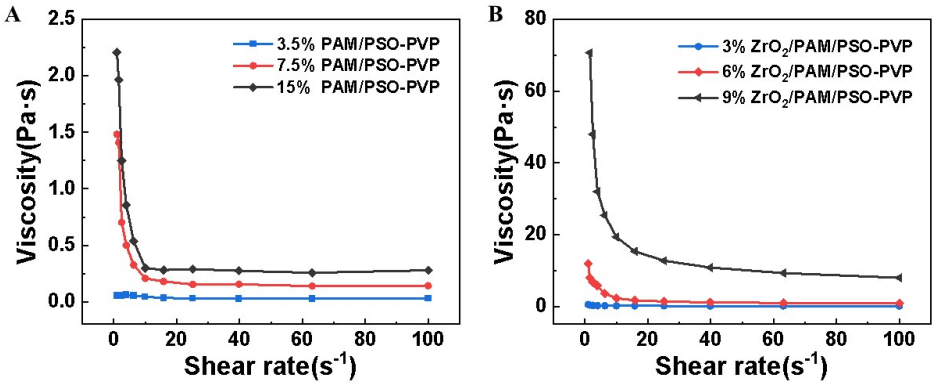

Figure S1 Viscosity of mullite and ZrO_2@Mullite precursor solutions: (A) PAM/PSO-PVP; (B) ZrO_2/PAM/PSO-PVP

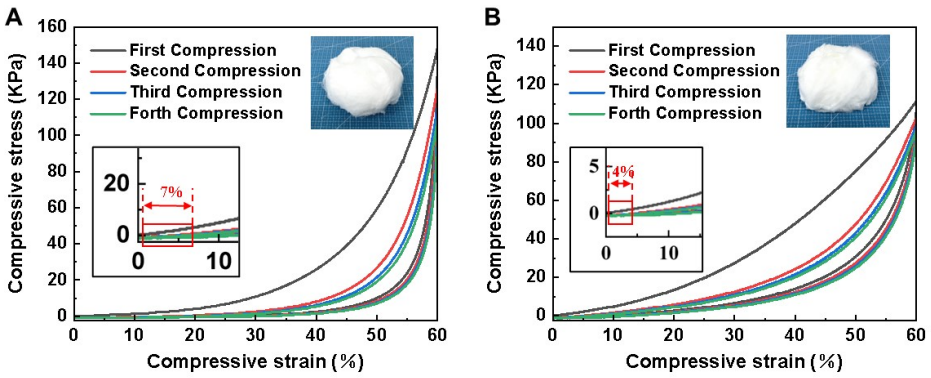

Figure S2 (A) Mullite precursor nanofibers and compression of mullite fibrous aerogels at 60% strain; (B) ZrO_2@Mullite precursor nanofibers and compression of ZrO_2@Mullite fibrous aerogels at 60% strain

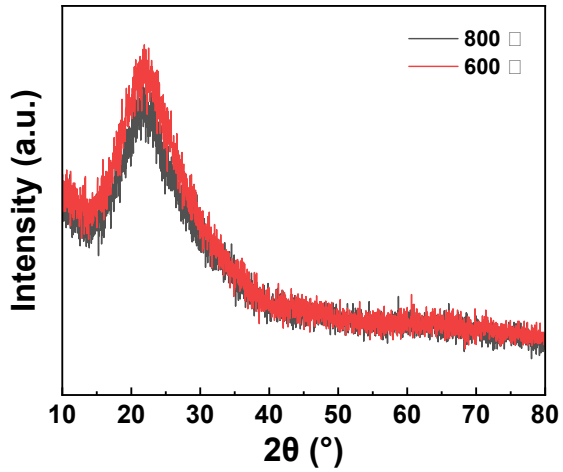

Figure S3 XRD of mullite nanofibers at 600 °C and 800 °C

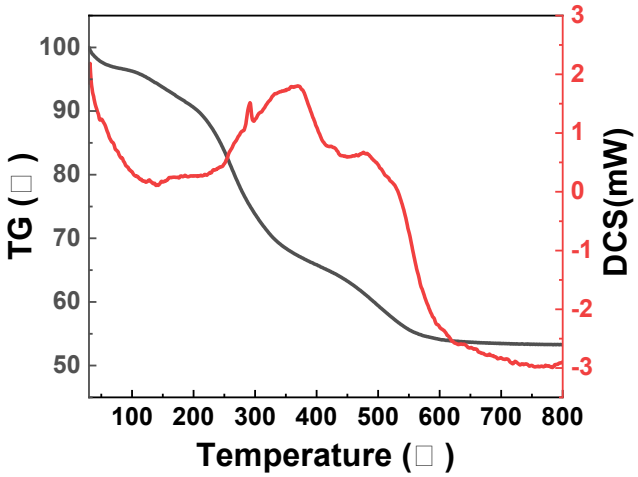

Figure S4 Thermogravimetric of mullite nanofibers at 800 °C

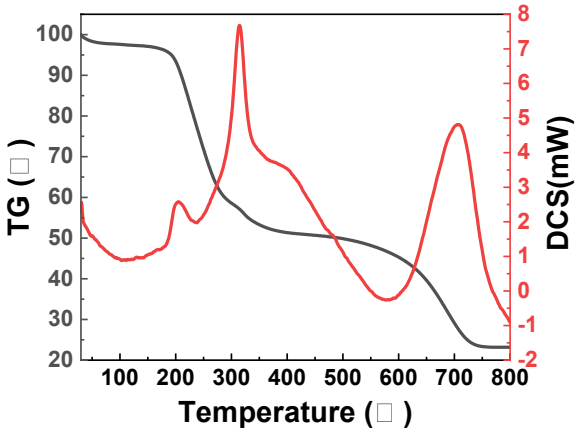

Figure S5 Thermogravimetric of ZrO_2@Mullite nanofibers at 800 °C

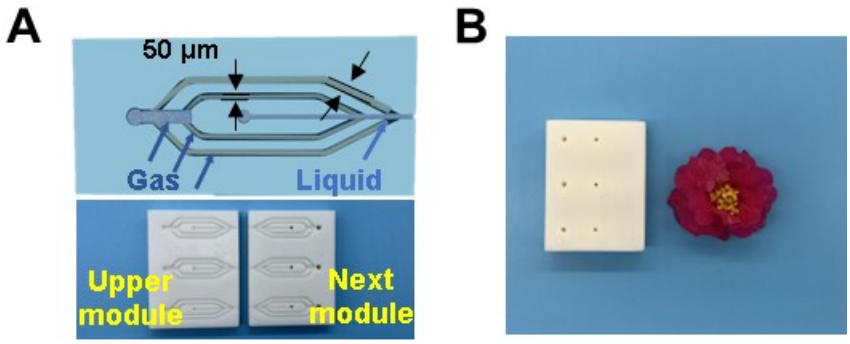

Figure S6 The structure of the microfluidic device: (A) the microstructure and physical diagram of the microfluidic device; (B) Size of microfluidic device

Figure S7 The lightweight ZrO_2@Mullite nanofibrous aerogels can be placed on the stamens

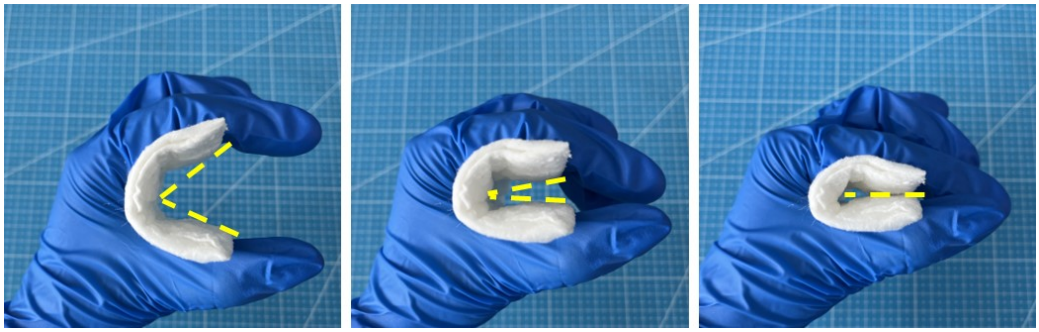

Figure S8 ZrO_2@Mullite nanofibrous aerogels with different curvature

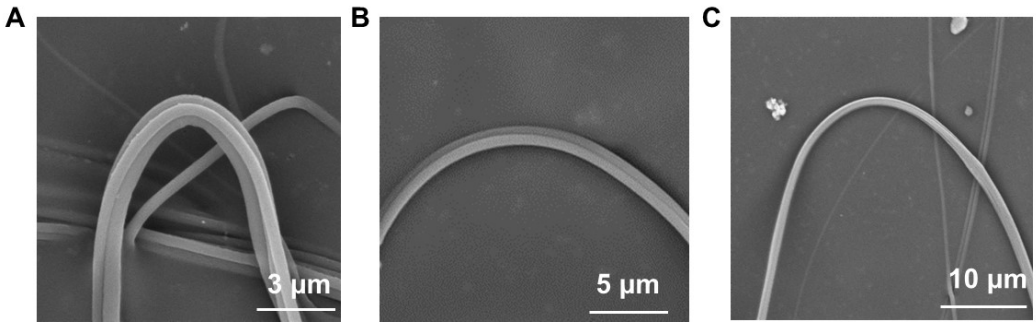

Figure S9 Microstructure of different bending nanofibers: (A) fiber bundles; (B) A small number of curved nanofibers; (C) Single curved nanofiber

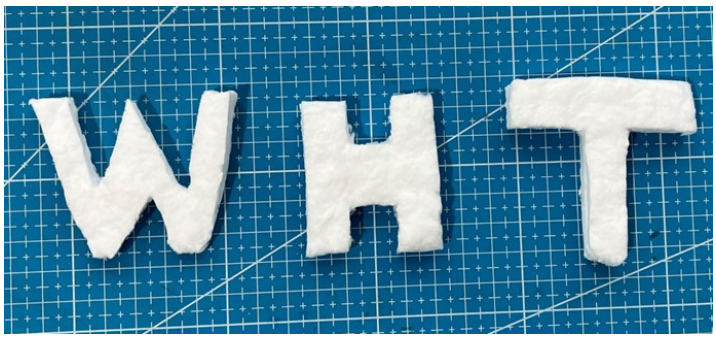

Figure S10 ZrO_2@Mullite nanofibrous aerogels with different morphologies

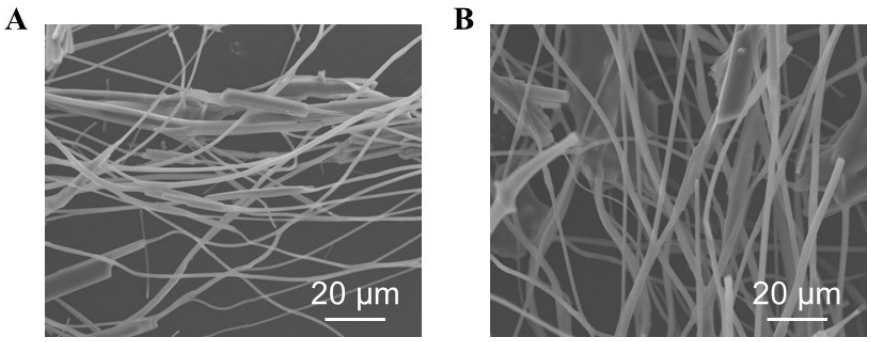

Figure S11 Microstructures of different fiber orientations: (A) 0°; (B) 90°

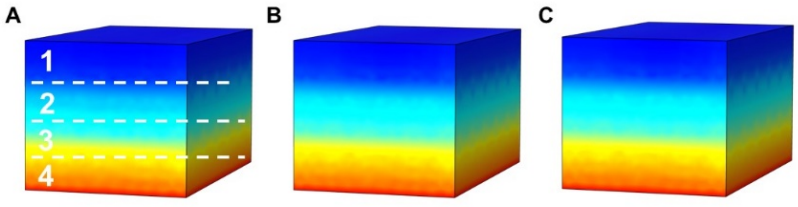

Figure S12 The temperature change of ordered lamellar ZrO_2@Mullite nanofibrous aerogel at different time: (A) 10s; (B) 30 s; (C) 50s

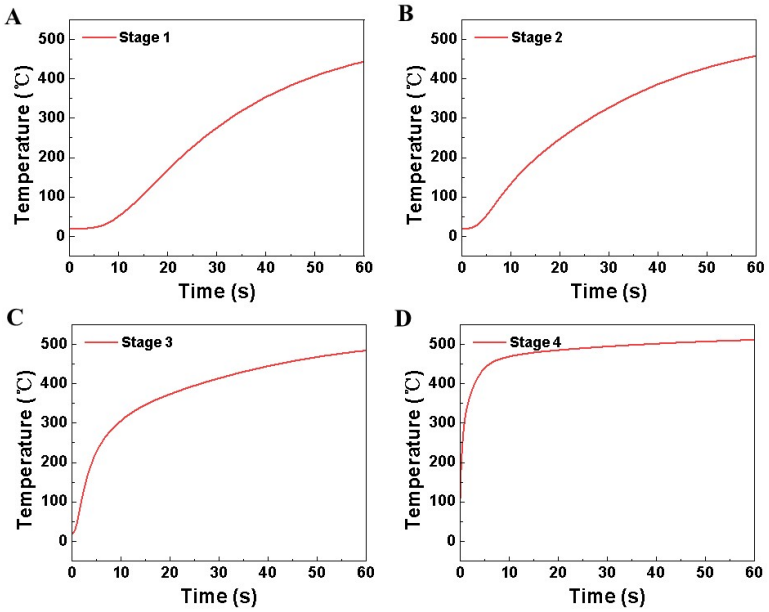

Figure S13 The temperature change curves of ordered lamellar fibrous aerogels at four stages: (A) Stage 1; (B) Stage 2; (C) Stage 3; (D) Stage 4

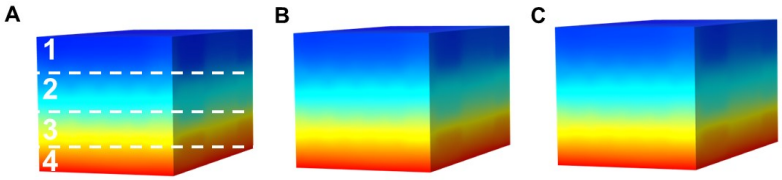

Figure S14 The temperature change of disordered lamellar ZrO_2@Mullite nanofibrous aerogel at different time: (A) 10s; (B) 30 s; (C) 50s

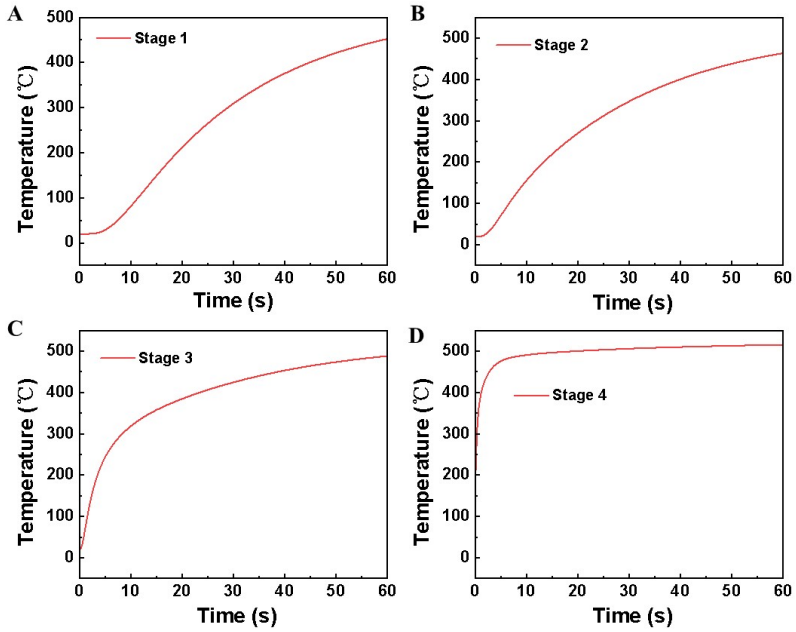

Figure S15 The temperature change curves of disordered lamellar fibrous aerogels at four stages: (A) Stage 1; (B) Stage 2; (C) Stage 3; (D) Stage 4

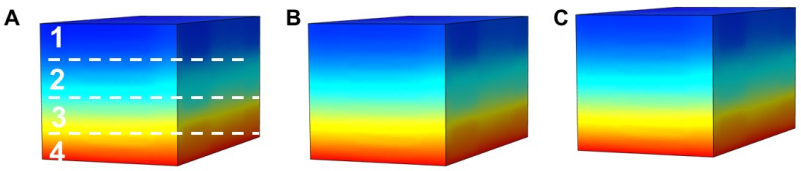

Figure S16 The temperature change of disordered ZrO_2@Mullite nanofibrous aerogel at different time: (A) 10s; (B) 30 s; (C) 50s

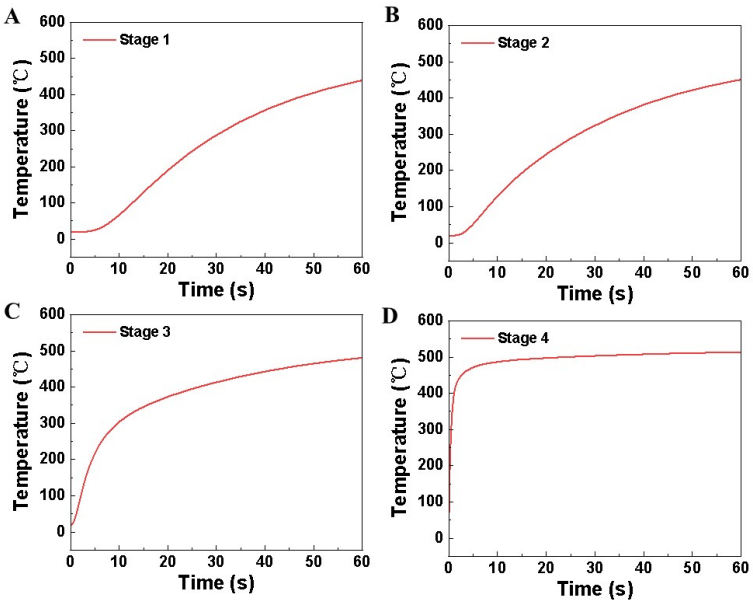

Figure S17 The temperature change curves of disordered fibrous aerogels at four stages: (A) Stage 1; (B) Stage 2; (C) Stage 3; (D) Stage 4

Figure S18 The thermal insulation of ZrO_2@Mullite nanofibrous aerogels